JOURNAL OF CATALYSIS 125, 9–34 (1990)

Morphology of Nickel Supported on Silica, Niobia, and Binary Oxide Thin Films

J. G. WEISSMAN,[1] E. I. KO,[2] AND P. WYNBLATT*

*Department of Chemical Engineering and *Department of Metallurgical Engineering and Materials Science, Carnegie Mellon University, Pittsburgh, Pennsylvania 15213*

Received August 4, 1989; revised December 6, 1989

Nickel deposited by radio-frequency sputtering onto single oxide, SiO_2 and Nb_2O_5, and binary oxide, Nb_2O_5–SiO_2 surface oxide and Nb_2O_5/SiO_2 mixed oxide, thin films was studied by transmission electron microscopy and selected-area diffraction after reduction in H_2 at 300, 500 or 650°C for up to 4 h. The use of thin films permitted a qualitative and quantitative analysis of the behavior of Ni supported on the various oxides. Observation of the oxide supports showed that the specific environment of niobia significantly affected its mobility. The behavior of Ni depended mostly on the interaction with Nb_2O_5 species and to a lesser extent on the interaction of nickel oxide with the support. These results were combined with chemical kinetic data on similar high-surface-area samples to develop a model based on various oxide–oxide and oxide–metal interactions for the behavior of supported nickel catalysts.

INTRODUCTION

The physical and chemical behavior of Group VIII metals supported on reducible oxides is now well understood (*1, 2*). After an appropriate reduction, an interaction between the metal and support is observed which is referred to as a strong metal–support interaction. This interaction is thought to arise from the migration of reduced oxide moieties, derived from the support, onto the surface of the supported metal particles, either by surface migration and/or bulk diffusion through the metal particle. The reduced oxide species modify the catalytic properties of the supported metal by physically blocking some reaction sites and creating new sites with different properties by local electronic interactions.

In the past several years our laboratory has shown that by modifying the environment of the reducible oxide, in our case either Nb_2O_5 or TiO_2, the extent and nature of metal–support interaction can be modified (*3–6*). For example, when nickel is supported on a surface oxide consisting of either Nb_2O_5 (*3*) or TiO_2 (*6*) on SiO_2, a decreased availability of the interaction oxide, coupled with an interaction between the support and supporting oxide, resulted in a lowered mobility of the interacting species. Work in our laboratory has since been extended to Nb_2O_5/SiO_2 mixed oxides with the two components homogeneously distributed in the bulk. As shown in Table 1, the behavior of chemical probes on Ni, after reduction at 500°C for 1 h, is strongly dependent on the support used, be it single, surface, or mixed oxide. More specifically, while Ni on the SiO_2 support behaves in what is considered a normal manner and Ni on the Nb_2O_5 support behaves as in the strong metal–support interaction model, the chemistry of Ni on the two niobia–silica binary oxide supports is not what would be expected from either of the two component oxides. All of the niobia-containing supports show a reduced H_2 chemisorption capacity, yet the turnover frequency for CO hydrogenation varies greatly, being lowered on the mixed oxide (NS50 and NS75) supports, while enhanced on the Nb_2O_5 support and

[1] Present Address: Texaco, Inc., P.O. Box 509, Beacon, NY 12508.

[2] To whom correspondence should be addressed.

0021-9517/90 $3.00

TABLE 1

Kinetic Data for Nickel on Various Supports[a]

Support	H_2 chemisorption H/Ni[b]	CO hydrogenation	
		N_{CO}[c]	% C_1[d]
SiO_2	1.0[e]	0.024[e]	83.[e]
NSI[f]	0.14[g]	0.170[g]	58.[g]
NS50[h]	0.12[e]	0.006[e]	79.[e]
NS75[h]	0.07[e]	0.017[e]	80.[e]
Nb_2O_5	0.02[i]	0.058[i]	51.[i]

[a] After reduction at 500°C, 1 h; all supports contain 9–10 wt% Ni.

[b] Measured by pulse chemisorption.

[c] Measured at 275°C, given as molecules/(surface Ni atom)/s.

[d] As mole percentage of product, measured at 211°C, except NSI, measured at 187°C.

[e] Taken from Ref. (*46*).

[f] Niobia–silica surface oxide.

[g] Taken from Ref. (*3*).

[h] Nomenclature refers to 50 or 75 wt% niobia, remainder silica.

[i] Taken from Ref. (*4*).

even more so on the surface oxide (NSI) support, compared to the SiO_2 support. The selectivity towards C_1 production is essentially unchanged in going from SiO_2 to mixed oxide supports, yet is reduced for the surface oxide and Nb_2O_5 supports.

In a support containing two oxides, oxide–oxide interactions play a key role in determining the resultant metal–support interactions. The use of low-surface-area samples to model high-surface-area catalysts has been successfully demonstrated for systems containing a single oxide (*7, 8*). More recently, model thin films have been used to study the behavior of supported oxides (*9, 11*). In this work we focus on the combined issues of oxide–oxide and metal–oxide interactions by studying Ni on binary oxide thin film supports, an area little treated in the literature. In addition to using the SiO_2 and Nb_2O_5–SiO_2 thin films studied previously in our laboratory, we prepared two new thin films for this study, a Nb_2O_5/SiO_2 mixed oxide thin film and a Nb_2O_5 thin film. These films were calcined for up to 1000°C or reduced at 500°C for 1 h, and then observed by electron microscopy, enabling observation of phase and structure changes inherent in the supporting oxides. Nickel was deposited onto the four thin films by radio-frequency sputtering and then reduced in hydrogen at 300, 500 and 650°C for either 1 or 4 h, followed by observation of the nickel-containing thin films by electron microscopy. Our intent is not to characterize the chemical properties of these films but rather, through structural studies on nickel as well as the binary oxide supports, to elucidate the complex catalytic behavior previously found for their high-surface-area counterparts. Particular emphasis will be placed on the influence of interactions between the two supporting oxides and with the supported metal on the structural characteristics of these samples.

EXPERIMENTAL PROCEDURES

Sample preparation. Approximately 80-nm-thick SiO_2 films were prepared by first evaporating silicon onto NaCl crystal cleavage fragments under a high vacuum. The salt was removed by dissolution in water; the released flakes of silicon were then picked up onto stainless-steel transmission electron microscopy grids. These were oxidized at 1000°C for 4 h, producing a homogeneous, nearly amorphous SiO_2 thin film. Niobia was deposited onto some silica thin films by radio-frequency sputtering inside a chamber held at about 6 Pa of an argon–oxygen mixture, resulting in reactively sputtered films close to Nb_2O_5 in composition. The films were fully oxidized to Nb_2O_5 after exposure to atmosphere. The morphology and behavior of the silica films and the niobia–silica surface oxide films have been described in detail (*10, 11*).

Niobia and niobia–silica mixed oxide thin films were prepared by radio-frequency sputtering using previously described equipment (*10, 11*). Targets consisted of either a disk of pure niobium metal or, for production of a mixed oxide thin film, a disk of pure

TABLE 2

Phases Observed in Thin Film Supports by Selected-Area Diffraction[a]

Treatment	SiO_2[b]	NSI	NS68	Nb_2O_5
(500,2,O)	A	T[c]	A[d]	T
(600,2,O)	A	T	—	T
(600,16,O)	A	T + H[e]	—	(T + B)[f]
(800,2,O)	A	—	T	—
(1000,—,O)	A	—	T + H[e]	(H + M)[f]
(500,2,O) + (500,1,H)	A	T[c]	T[e]	A[d]

[a] Some phases abbreviated by: T, TT or T-Nb_2O_5; B, B-Nb_2O_5; M, M-Nb_2O_5; H, H-Nb_2O_5; A, amorphous.

[b] Pretreated at (1000,4) to fully oxidize film.

[c] Previously identified by HRTEM (*16*).

[d] Probably contains TT- or T-Nb_2O_5 crystals too small to contribute significant intensity to diffraction pattern.

[e] Comparatively weak diffraction intensity.

[f] Complex diffraction pattern precludes positive identification.

silicon placed on top of the disk of niobium. Varying the ratios of exposed surface areas of the two metals was used to adjust the as-deposited composition of the film. Sputtering was done in an inert atmosphere of argon to facilitate sputtering rates. The deposition substrate was approximately 20-nm-thick carbon film supported on a stainless-steel 200-mesh transmission electron microscopy grid. Enough niobium or niobium/silicon mixture was deposited to give a final thickness of about 80 nm after full oxidation. After sputter deposition, all four thin films were oxidized at 500°C for 2 h. These films were subsequently oxidized under various conditions as listed in Table 2, similar to those used to calcine corresponding high-surface-area samples (*12, 13*). In addition, the four thin film samples were reduced for 1 h in a tube furnace at 500°C in flowing hydrogen.

Nickel was deposited onto the four thin film supports using radio-frequency sputtering as described above. The target was a disk of pure nickel, and sputtering was done in argon. Enough nickel was deposited to produce a film of about 0.9 nm equivalent thickness. After deposition, the nickel-containing films were reduced in flowing hydrogen at 300, 500, or 650°C for either 1 or 4 h.

All thin film samples were examined by transmission electron microscopy using a Philips 420 electron microscope operating at 120 KV, and having a line-to-line resolution of about 0.4 nm. Phase identifications were obtained by taking selected-area diffraction patterns of appropriate regions on the samples. Some thin films were analyzed by energy-dispersive spectroscopy (EDS) using a CAMSCAN scanning electron microscope and a Princeton Gamma-Tech Si(Li) detector. The micrographs presented in this paper illustrate several contrast mechanisms, including contrast arising from varying film thickness, varying electron defocus, and degree and size of crystallization. Care should be exercised in interpreting micrographs containing multiple contrast features (*14*).

RESULTS

Thin film supports. The appearances of the four different thin film supports, silica, niobia–silica surface oxide, niobia–silica mixed oxide, and niobia, after heat treatment at 500°C for 2 h in oxygen are depicted in Fig. 1. The two films containing silica and niobia were found to be spatialy uniform by EDS mapping. For convenience, these films will be designated at SiO_2, NSI, NS68, and Nb_2O_5, with treatment conditions given in the form (temperature in °C; time in hours; heat treatment atmosphere: O indicates oxygen or air, H hydrogen). As an example, Fig. 1A is of (500,2,O)SiO_2, or a SiO_2 thin film heated at 500°C for 2 h in oxygen. Phases observed by selected-area diffraction in these films after various heat treatments are given in Table 2. For comparison, phases found by X-ray or selected-area electron diffraction for the high-surface-area or bulk supports are given in Table 3.

The behavior of SiO_2 and NSI films has been discussed previously (*10, 11*). Silica thin films were found to remain amorphous and nearly homogeneous up to calcining

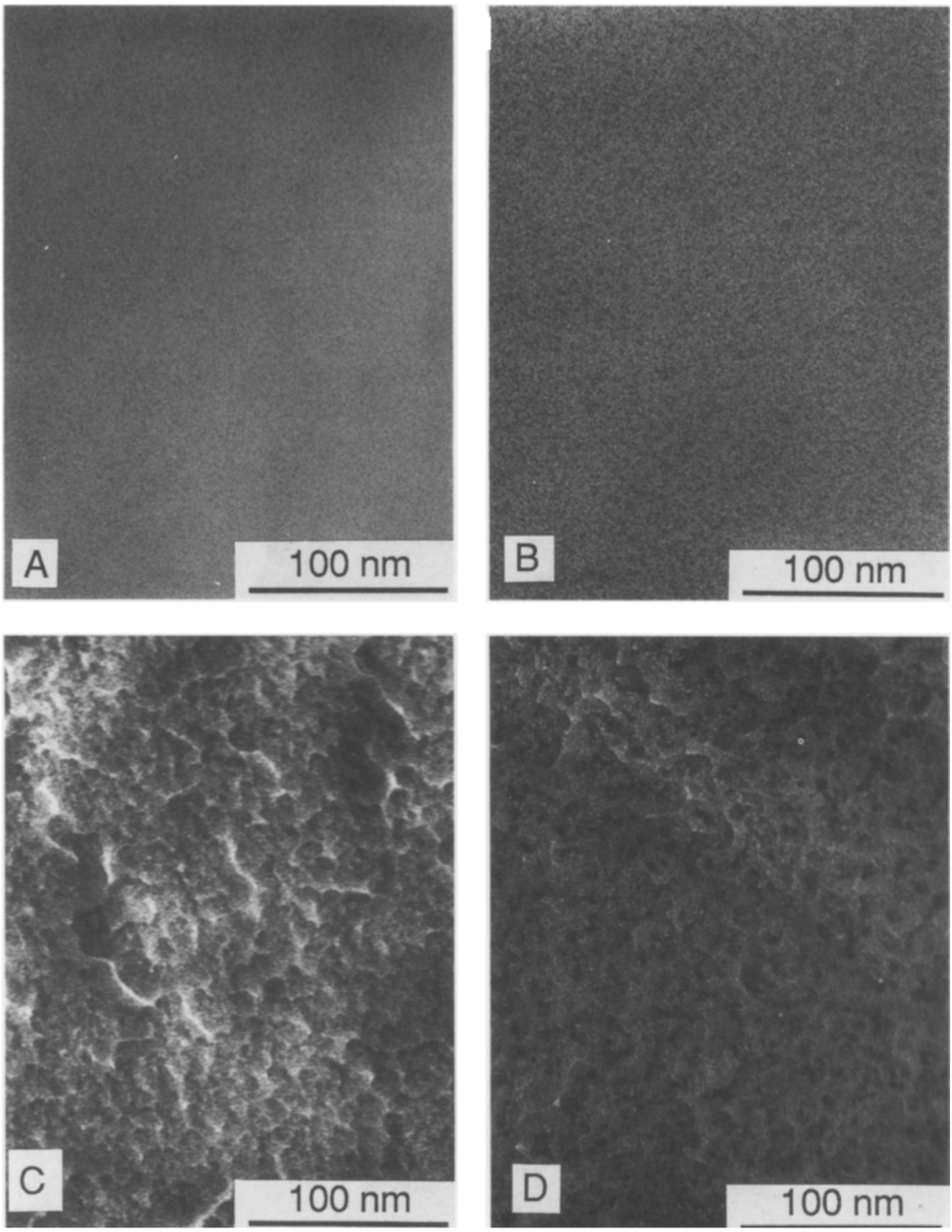

FIG. 1. Micrographs of single and binary oxide thin film supports after treatment in air at 500°C for 2 h. A, SiO_2; B, NSI; C, NS68; D, Nb_2O_5. The contrast seen in B is due to microcrystalline T-Nb_2O_5, while the contrast seen in C and D is due to a combination of thickness and mass contrast, including some contrast arising from incipient niobia crystallization.

TABLE 3

Phases Observed in High-Surface-Area Supports or Bulk Materials[a]

Treatment	NSI[b]	NS50[c]	NS75[c]	Nb_2O_5[b,c]	Nb_2O_5[d]
(500,2,O)	A	A	A	T	T
(600,2,O)	A	—	—	T	T
(600,16,O)	T	—	—	—	T
(800,2,O)	T	T	T	T	T + B
(1000,—,O)	T	T	T	T	B + H
(1000,48,O)	T	T + H	T + H	H	H

[a] Some phases abbreviated by: T, TT or T-Nb_2O_5; B, B-Nb_2O_5; H, H-Nb_2O_5 or a similar phase such as M-Nb_2O_5; A, amorphous.

[b] Obtained by selected-area electron diffraction.

[c] Obtained by X-ray diffraction, taken from Ref. (*12*).

[d] Obtained by X-ray diffraction, taken from Ref. (*15*).

temperatures of 1000°C, retaining the appearance of Fig. 1A. NSI films were found to consist of niobia in two states on the surface, strongly held to silica via niobium–oxygen–silicon bonds, or crystallized as small (1–2 nm) crystals of metastable TT- or T-Nb_2O_5. Niobia has been found to occur in a wide range of forms, some of which are designated TT, T, B, M, and H. These forms differ in atomic structure and degree of crystallinity (*15*). Because of the difficulty in distinguishing the two closely related niobia forms of TT and T, they will be referred to as T-Nb_2O_5 throughout, although either TT- or T-Nb_2O_5 or both may occur (*16*). The darker contrast material in Fig. 1B corresponds to the T phase. As these films are heated for longer times or higher temperatures in air, T-Nb_2O_5 forms larger (10–20 nm) and more distinct crystals. Under the most extreme conditions studied (600,16,O), the stable H-Nb_2O_5 phase was observed to crystallize in addition to T-Nb_2O_5. These results are in contrast to what was found in the high-surface-area NSI supports (Table 3), which are amorphous under milder conditions and contain only T-Nb_2O_5 at the higher temperatures where the thin films were found to have H-Nb_2O_5. These differences in niobia behavior, having been found to arise from the much greater stabilization of surface niobia on high-surface-area silica, due to the significantly larger concentration of Nb–O–Si bonds capable of forming on the high-surface-area material (*10*), have been discussed in detail.

Both NS68 and Nb_2O_5 thin films appear amorphous after the initial oxidation at (500,2,O), as seen in Figs. 1C and 1D. These films have a much greater topological contrast compared to that of the SiO_2 or NSI films, probably due to the differences in preparation method of the two films. Energy-dispersive spectroscopy of the niobia–silica co-sputtered film indicates that the composition is 68% niobia by weight, thus the designation NS68. This is, by design, midway between two high-surface-area mixed oxide supports studied by our laboratory, NS50 and NS75. Upon further calcination, the NS68 film crystallizes first to T-Nb_2O_5 at (800,2,O) and then to a mixture of T- and what may correspond to H-Nb_2O_5 at (1000,—). This trend corresponds well to that of the high-surface-area NS50 and NS75 mixed-oxide samples (*12*). The phases identified in the niobia thin films corresponded closely to those reported in the literature (*15*). While the Nb_2O_5 film appeared to be amorphous at (500,2,O), increasing heat-treatment temperature resulted in a series of phases forming first T-, then B-, and finally H-Nb_2O_5, as illustrated in Fig. 2.

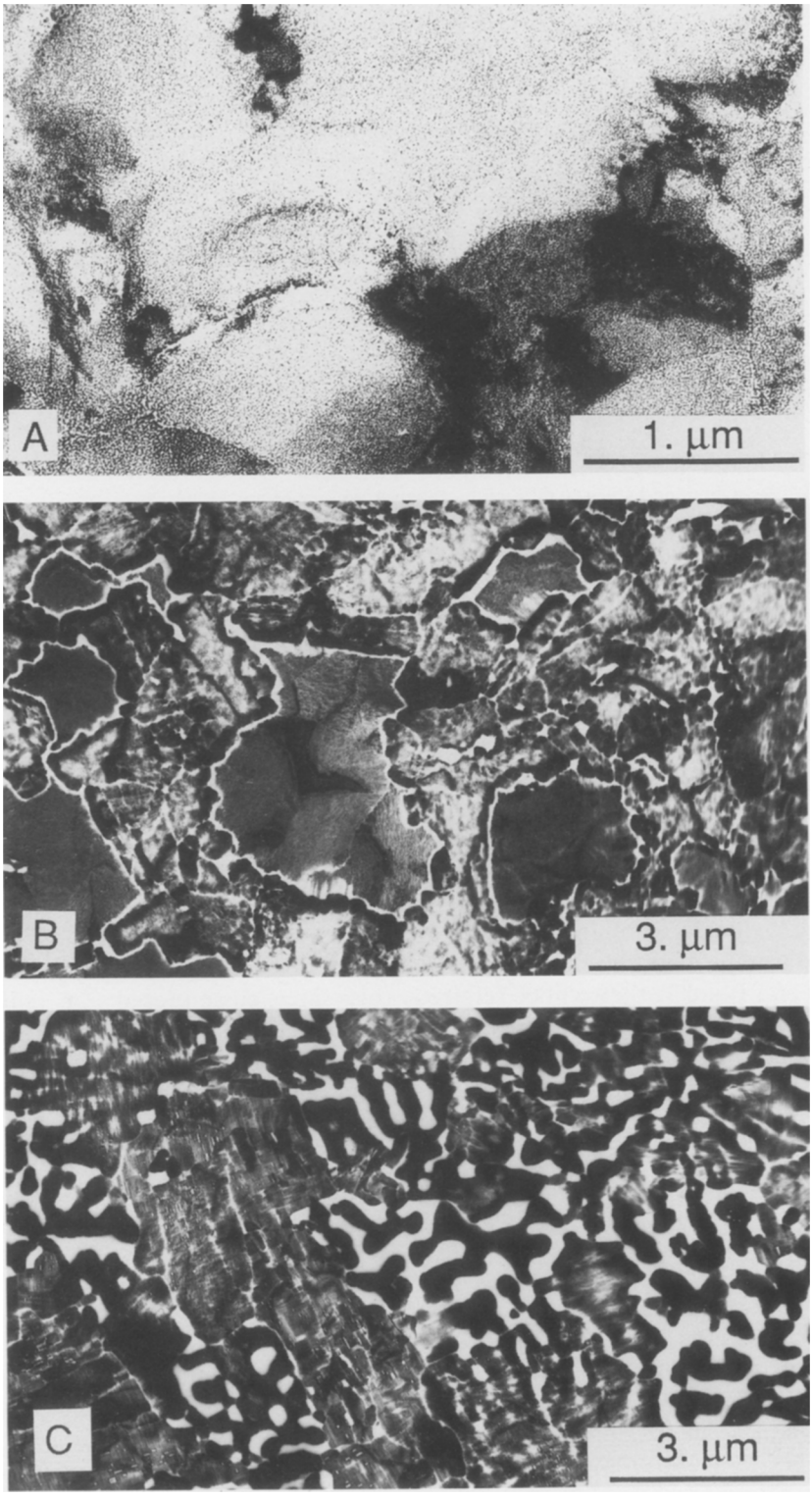

FIG. 2. Micrographs showing the effects of treatment in air on the crystallization and appearance of Nb_2O_5 thin films. A, 600°C for 2 h, containing T-Nb_2O_5; B, 600°C, 16 h, single-crystal regions are B-Nb_2O_5 connected by less distinct T-Nb_2O_5; C, heated to 1000°C, larger crystals are H-Nb_2O_5, connected by darker M-Nb_2O_5.

After oxidation at (500,2,O), the four thin film supports were exposed to reducing conditions (500,1,H), so that intrinsic changes due to H_2 exposure could be identified and separated from changes observed when nickel supported on the films was reduced, as described below. The apperances of the supports so treated are given in Figs. 3 and 4. No reduced phases, such as NbO_2, were noted in any of the niobia-containing films, either with or without nickel. Essentially no changes were observed in the SiO_2 and NSI films, as both had appearances similar to oxidized films (Fig. 1). While most portions of the NS68 thin film remained similar in appearance to unreduced films, continued heat treatment resulted in a slight increase in crystallization to T-Nb_2O_5 overall and the appearance of poorly crystallized aggregates in certain regions, as illustrated in Fig. 4A. The aggregates are roughly round in outline, and may represent more concentrated areas of T-Nb_2O_5 crystallization. The niobia thin film showed more dramatic changes due to H_2 treatment. Numerous contrast features having the appearance of pits or holes can be clearly seen in Fig. 3D, together with the development of darker contrast regions. This is more clearly noted in Fig. 4B, where in addition to the pits, larger crystals having a morphology similar to that of H-Nb_2O_5 appear, even though electron diffraction from these crystals was too weak to contribute to the observed pattern. The formation of pits in reducible oxide supports has also been noted in the case of rutile (TiO_2) thin films (*17, 18*).

Supported nickel. As-deposited nickel, having a thickness equivalent to about 0.9 nm for a uniform thin film, generally consisted of small particles of the isometric form of nickel oxide. The appearance of NiO particles on the four supports discussed above is given in Fig. 5, most clearly seen in Figs. 5A and 5B. NiO particles could not be observed on the NS68 and Nb_2O_5 supports due to the high contrast of the support; however, NiO was detected by selected-area electron diffraction on Nb_2O_5, but not on NS68 due to intense amorphous scattering.

Films treated for 1 h in hydrogen at 300, 500 and 600°C are illustrated in Figs. 6, 7, and 8, while films treated for 4 h at the same temperatures are illustrated in Figs. 9, 10, and 11. Phases found by selected-area electron diffraction on the as-deposited and reduced supported Ni films are given in Table 4. On the high-silica-content supports, SiO_2 and NSI, NiO was not reduced to Ni until reduction temperatures over 300°C were employed. At a reduction temperature of 650°C and on the NSI supports, a phase observed by selected-area diffraction, probably corresponding to either $Ni_{0.67}Nb_{11.33}O_{29}$ or $NiNb_2O_6$, was found from comparison with published diffraction data (*19*). A similar result was found by Hu *et al.* (*20*) when a niobia surface oxide was calcined on Ru/SiO_2 at 700°C, forming $RhNbO_4$. In both cases, a high-temperature heat treatment caused the formation of a compound, either $NiNb_2O_6$ or $RhNbO_4$, that is fully oxidized regardless of the atmosphere. All crystalline niobia phases observed in this study were found to be fully oxidized; however, reduced niobia probably occurs in amorphous form as a surface oxide. Unlike previous work on NSI films not containing Ni (*10*), no evidence for T- or H-Nb_2O_5 identified earlier was found. This observation suggests that the interaction with Ni is affecting the crystallization of niobia by itself.

On the high-niobia-content supports, NS68 and Nb_2O_5, phase identification was complicated by the simultaneous crystallization of niobia. On some samples, T-Nb_2O_5 was noted in addition to Ni-containing phases; and in one instance, (650,1,H) Nb_2O_5, diffraction from crystallized niobia was sufficiently intense to obscure diffraction from Ni particles, although Ni could be observed on the sample (Fig. 8D). Only Ni was observed on the NS68 supports after reduction at 300°C, while Ni was observed on the Nb_2O_5 supports above 300°C reduction. At the lower reduction temperature, 300°C, phase identification on the Nb_2O_5

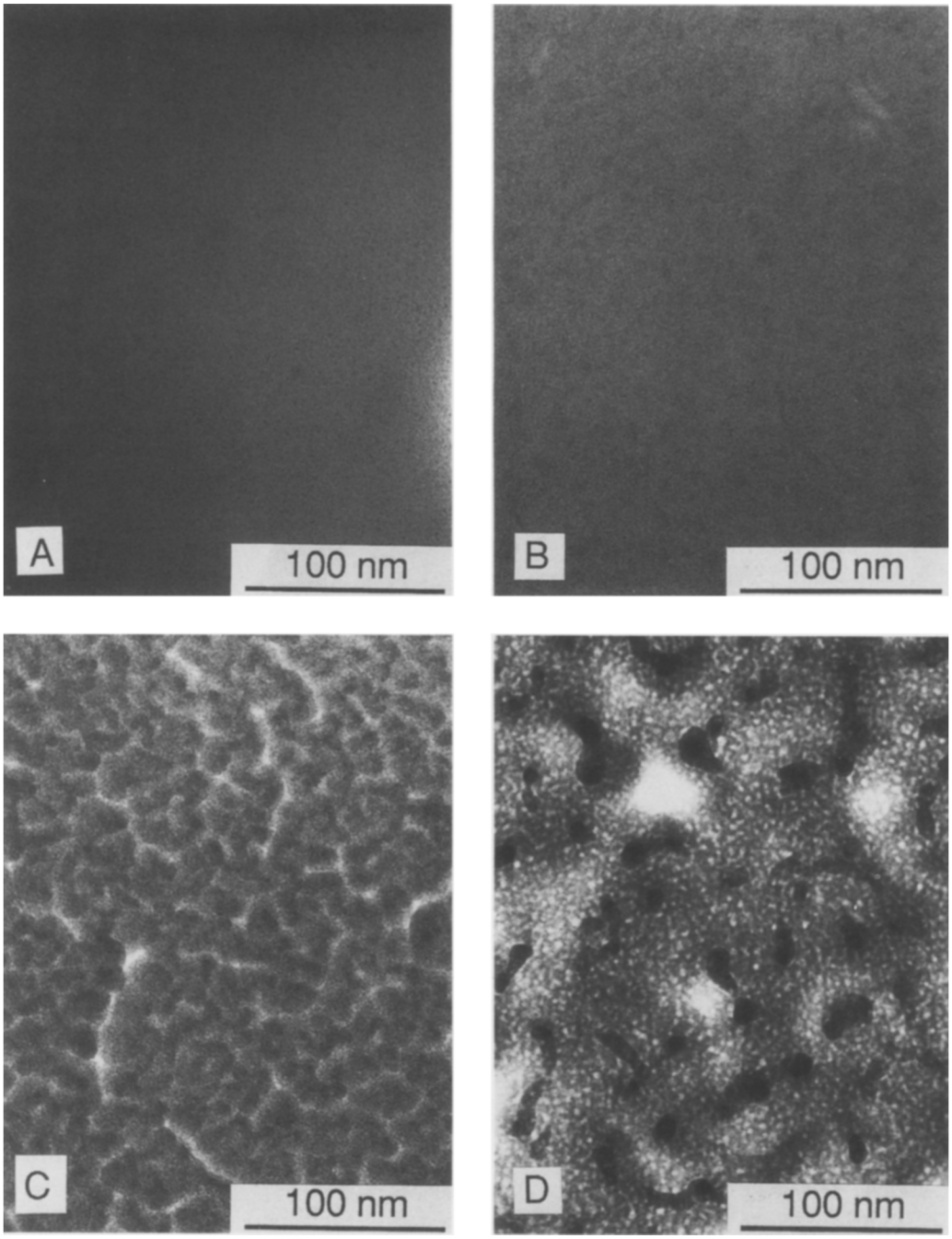

FIG. 3. Micrographs showing appearance of films illustrated in Fig. 1 after being reduced in H_2 for 1 h at 500°C. A, SiO_2; B, NSI; C, NS68; D, Nb_2O_5. Compared to Fig. 1, larger T-Nb_2O_5 crystals are apparent in B, and distinctly crystallized niobia is apparent in D.

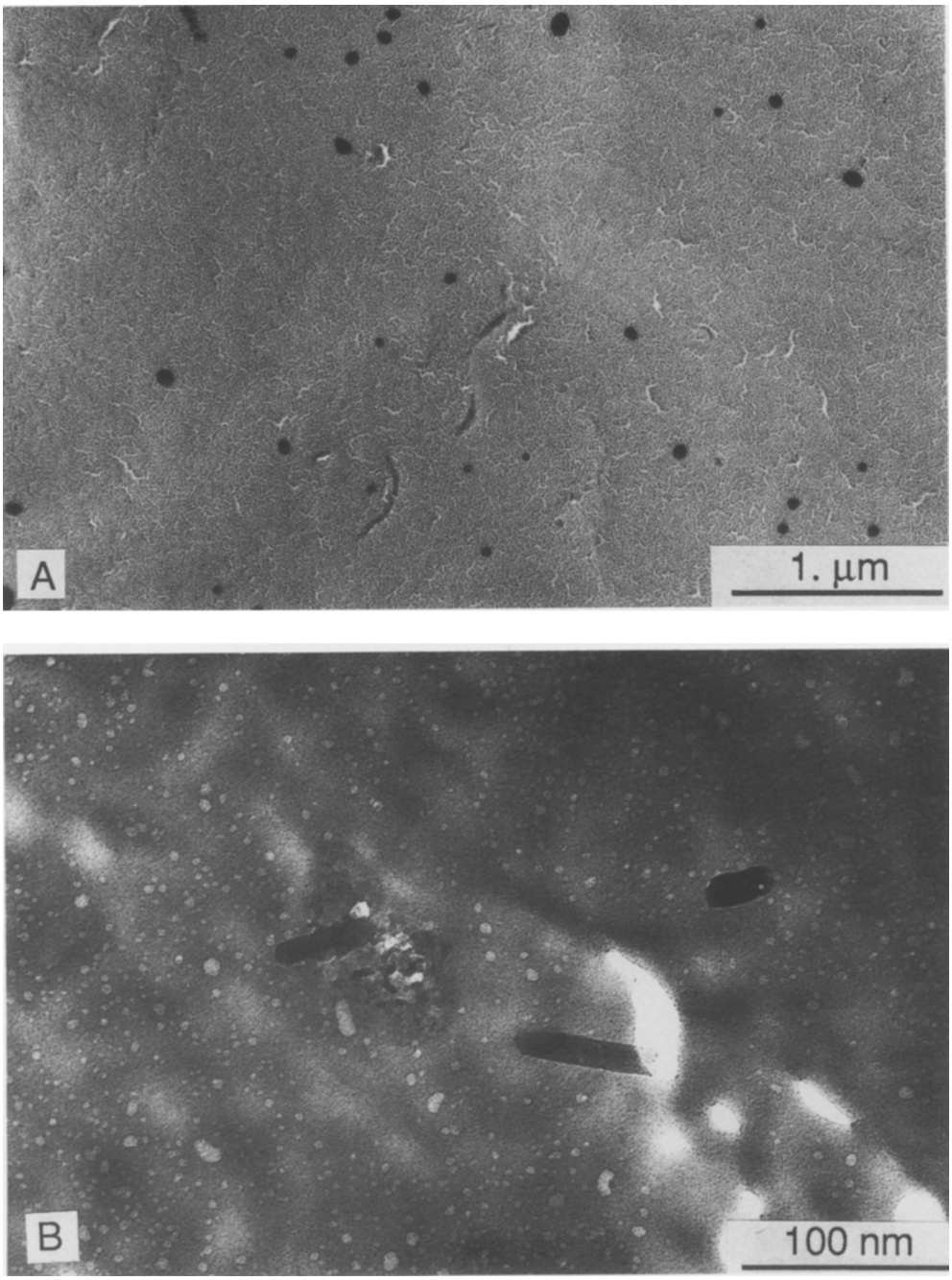

FIG. 4. Micrographs of different regions of NS68 and Nb_2O_5 films illustrated in Fig. 3, showing more extensive aggregation and niobia mobility in some areas of the films. Dark contrast features in A, NS68, are T-Nb_2O_5, while large crystals in B, Nb_2O_5, are similar in appearance to H-Nb_2O_5.

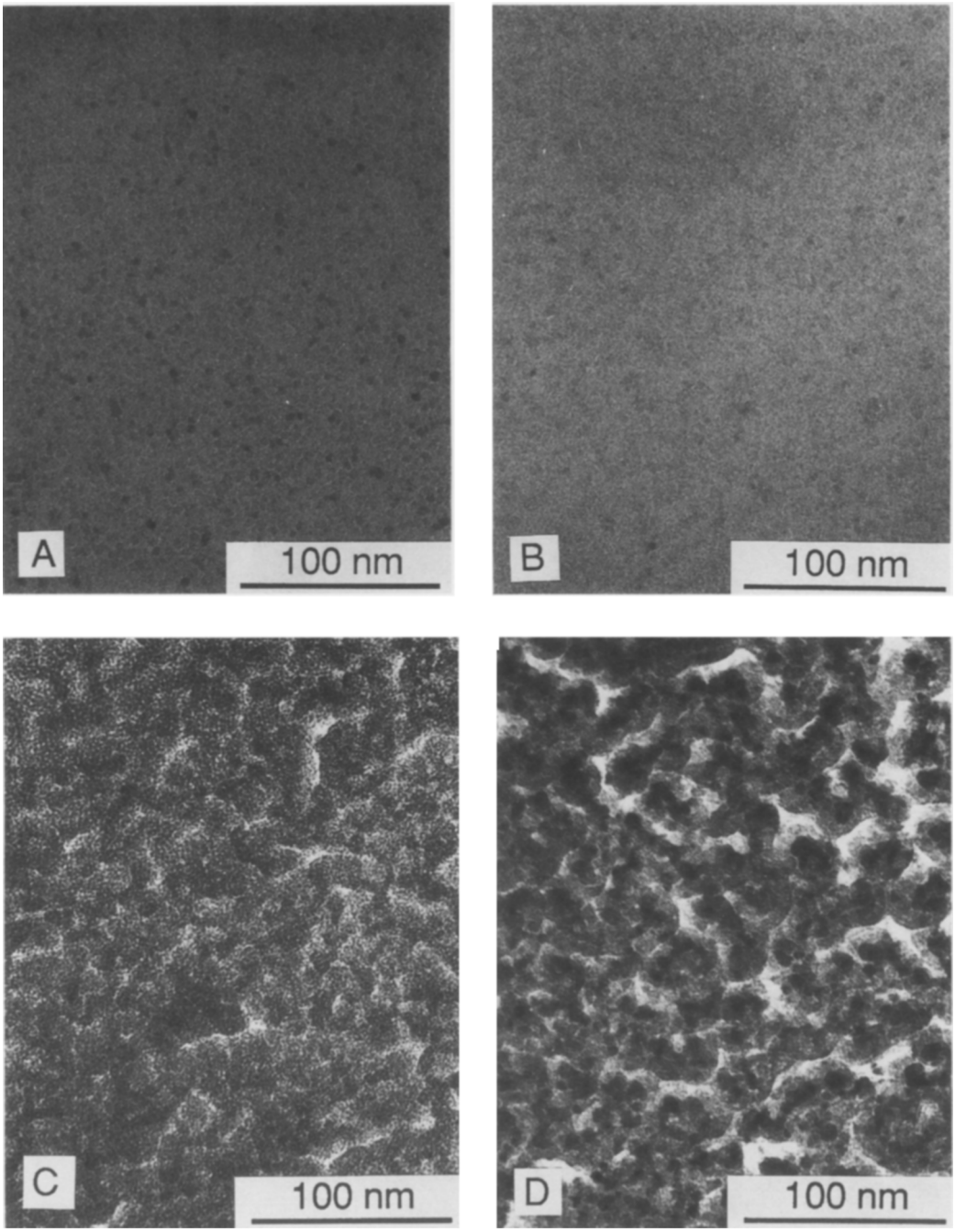

FIG. 5. Micrographs of the appearance of 0.9 nm equivalent thickness of Ni as deposited on the oxide films illustrated in Fig. 1. The supports are: A, SiO_2; B, NSI; C, NS68; D, Nb_2O_5. The darker contrast features in A are NiO crystals, which are only slightly apparent in B and not at all in C and D due to interfering contrast from the supports.

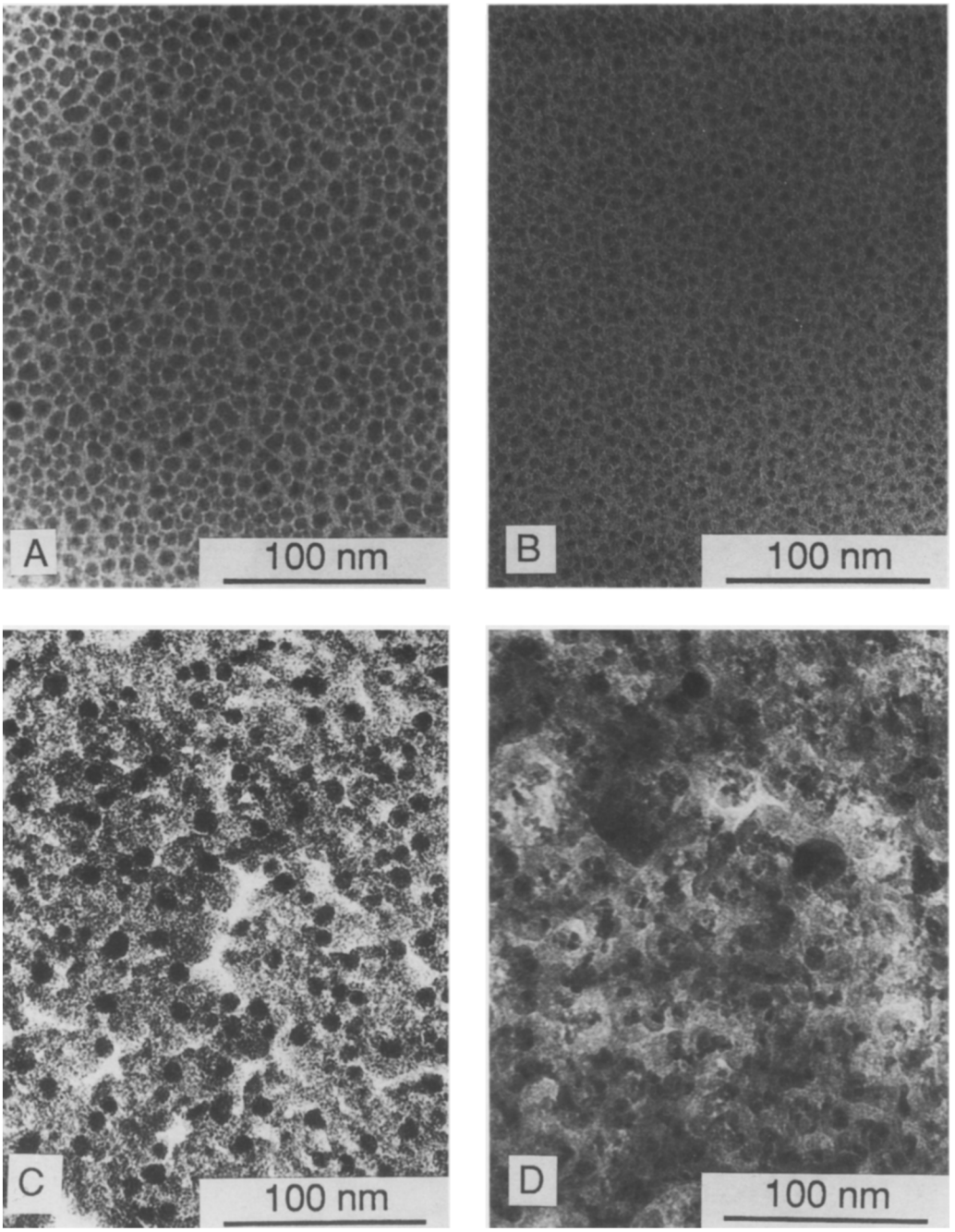

FIG. 6. Micrographs of the appearance of films illustrated in Fig. 5 after reduction in H_2 at 300°C for 1 h. Oxide supports are: A, SiO_2; B, NSI; C, NS68; D, Nb_2O_5. Ni crystals are not discernable in D due to high contrast of the support.

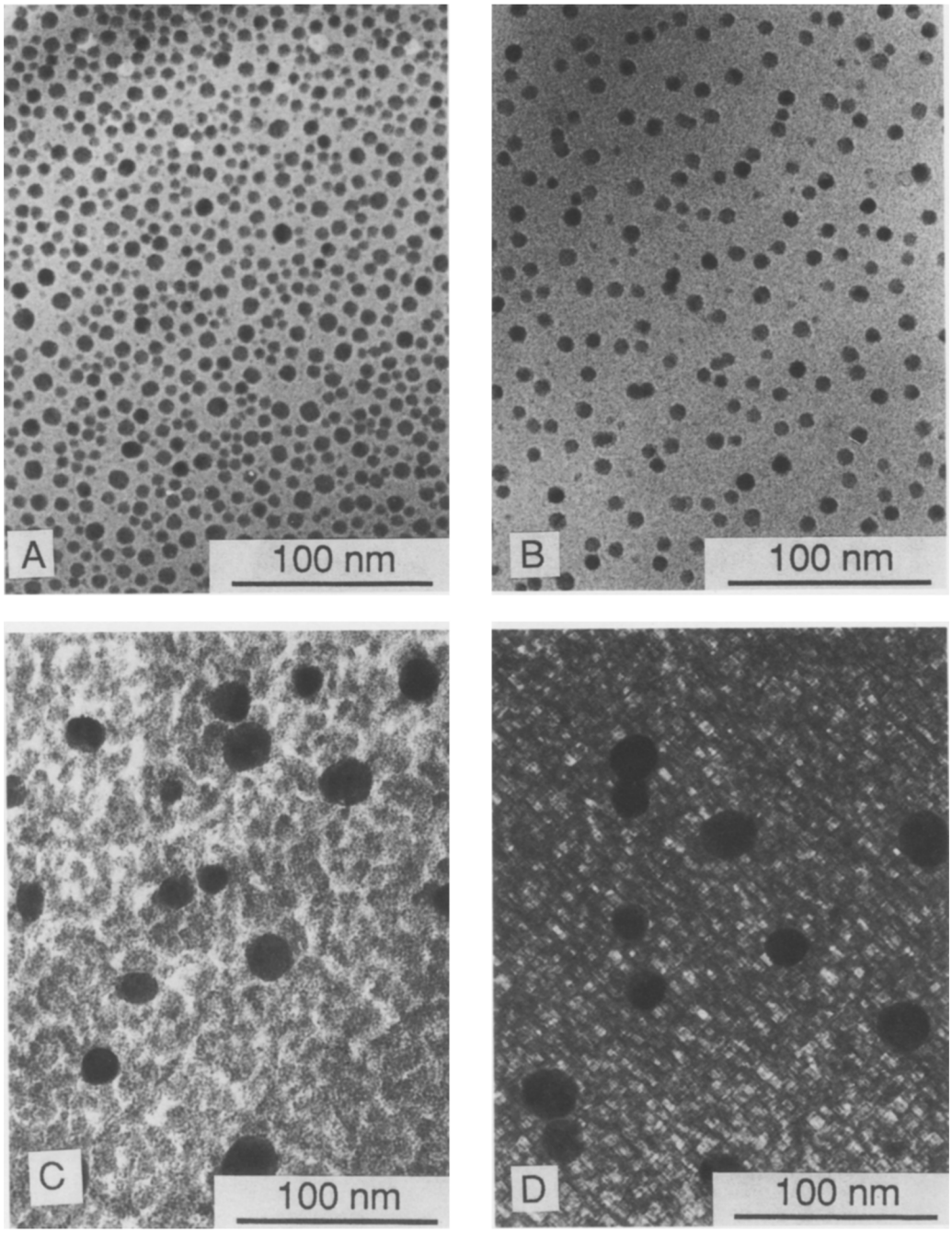

FIG. 7. Micrographs of the appearance of films illustrated in Fig. 5 after reduction in H_2 at 500°C for 1 h. Oxide supports are: A, SiO_2; B, NSI; C, NS68; D, Nb_2O_5. Crystallization of the support to T-Nb_2O_5 is apparent in D, the crystal illustrated having an (010) orientation.

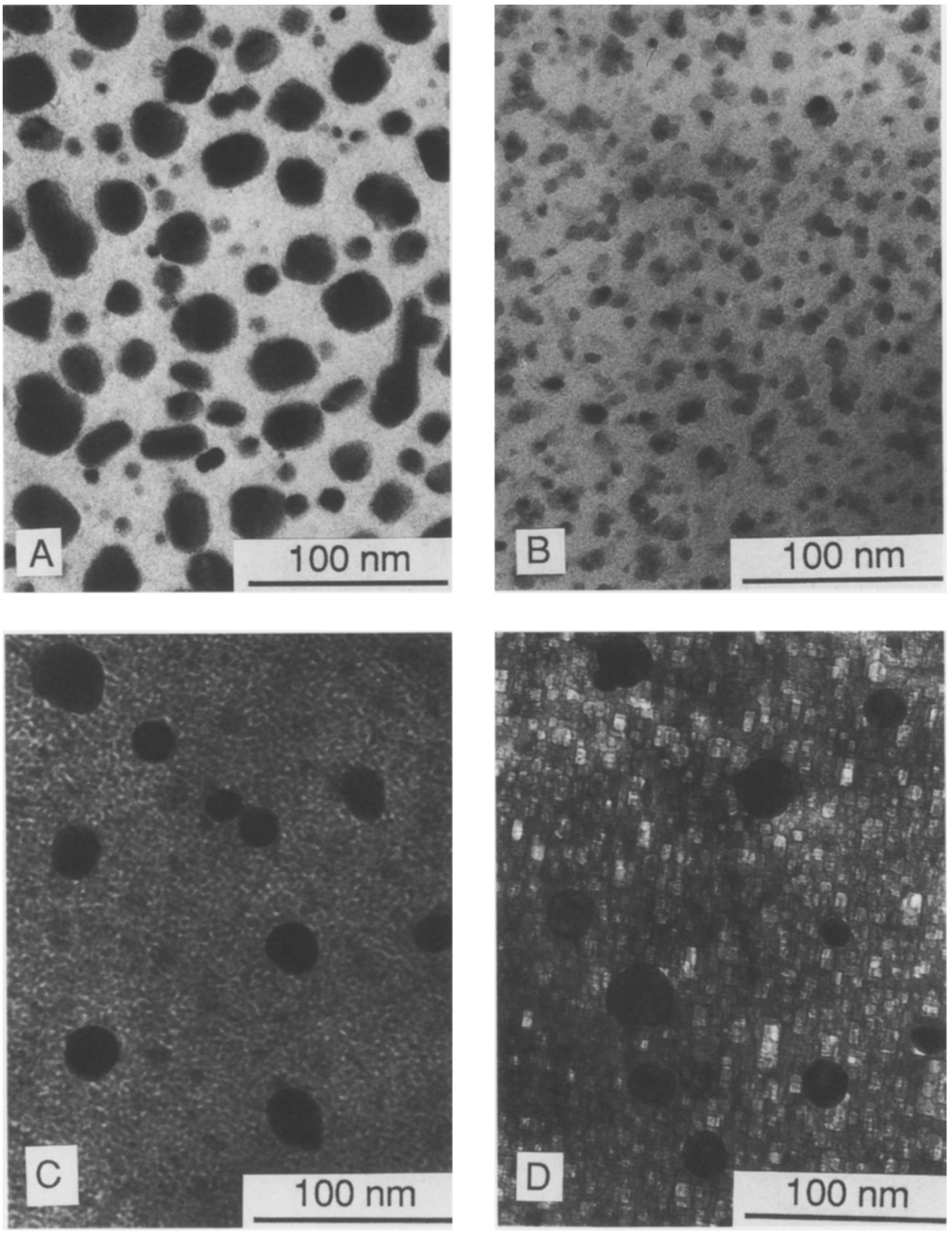

FIG. 8. Micrographs of the appearance of films illustrated in Fig. 5 after reduction in H_2 at 650°C for 1 h. Oxide supports are: A, SiO_2; B, NSI; C, NS68; D, Nb_2O_5. The support in D consists of relatively large T-Nb_2O_5 crystals; a portion of one having an (001) orientation is illustrated. The support in C contains microcrystalline T-Nb_2O_5 under these conditions.

supports was difficult due to the intense amorphous scattering of the support. Under the most extreme conditions (650,4,H), a nickel niobate was noted in addition to Ni and T-Nb_2O_5 on the Nb_2O_5 support. The presence of nickel niobate in nickel supported on high-surface-area niobia had been previously deduced by magnetic studies (*21*). An iron–niobia compound corresponding to $FeNbO_4$ was also noted after reduction of high-surface-area niobia-supported iron at 600°C for 16 h (*22*). Such a compound formation represents a severe form of metal–support interaction. Interestingly, nickel niobate was not observed on the NS68 support.

A careful examination of the various micrographs in Figs. 6–11 shows that there are significant variations in the appearances of nickel on the four supports, especially as higher reduction temperatures are reached. Because of the high contrast of the support, nickel particles in Figs. 6D and 9D were difficult to observe. For the other samples, average nickel particle diameters are given in Table 5 and particle size distributions for samples reduced for 1 h are given in Fig. 12. Distributions for samples reduced for 4 h were very similar in appearance, in agreement with the results of Table 5, as there is little significant variation in nickel particle diameters between the two reduction times. A similar behavior was found for Ni supported on γ-Al_2O_3 thin films (*23*). For samples reduced at 600 and 700°C for up to 20 h, no significant increases in particle diameter were noted between different reduction times; at least 45 h was needed for sintering to be observed.

NiO on SiO_2 appears as irregular shaped particles, even after reduction at 300°C. After 500°C reduction, nickel crystals on SiO_2 have a well-defined shape, the particles consisting, for the most part, of regular polyhedrons in projection, more easily observed in samples reduced at higher temperatures and longer times (Figs. 8A and 11A). Nickel on the NSI supports appear similar to nickel on SiO_2 at lower reduction temperatures, but significant particle spreading, more clearly illustrated in Fig. 13, is apparent after reduction at 650°C. This spreading corresponds to the occurrence of nickel niobate in diffraction patterns of the same samples; the lighter contrast regions surrounding the darker contrast nickel particles are probably this compound. The formation of nickel niobate in the NSI samples increased the difficulty of making measurements from the micrographs of these samples, as spreading of the oxide film leads to ambiguity in determining particle boundaries and to inaccuracies in measurements of both particle numbers and diameters. Nickel particles on NS68 and Nb_2O_5 appear similar, occurring on both supports as more-or-less well-formed crystals at lower reduction temperatures, but less well-defined and more round in projection at higher reduction temperatures. This behavior is clearly seen in Fig. 14 for samples treated at (650,4,H). Observations of identical regions of the nickel-containing films tilted at 45° and with no tilt indicated for the most part that Ni on the SiO_2, NS68, and Nb_2O_5 films were nearly equidimensional after reduction at 500 or 650°C. Particles on NSI observed by the tilting technique appeared to be more flat, although poor contrast between the particles and support in micrographs of the tilted samples made quantitative evaluation of aspect ratios difficult.

The average nickel particle diameters listed in Table 5 are somewhat larger than nickel particle diameters obtained on the corresponding high-surface-area samples treated under similar conditions (*3, 4, 24, 25*). This is to be expected as the per-surface-area loading on the thin films is higher than on the high-surface-area samples. However, the trend in particle diameters among the four supports is the same on both thin film and high-surface-area supports. Nickel particles are the smallest on SiO_2 and NSI (which give comparable sizes), larger on Nb_2O_5, and the largest on the mixed oxide supports.

DISCUSSION

Our results show that niobia exhibits a variety of behaviors whether alone or in dif-

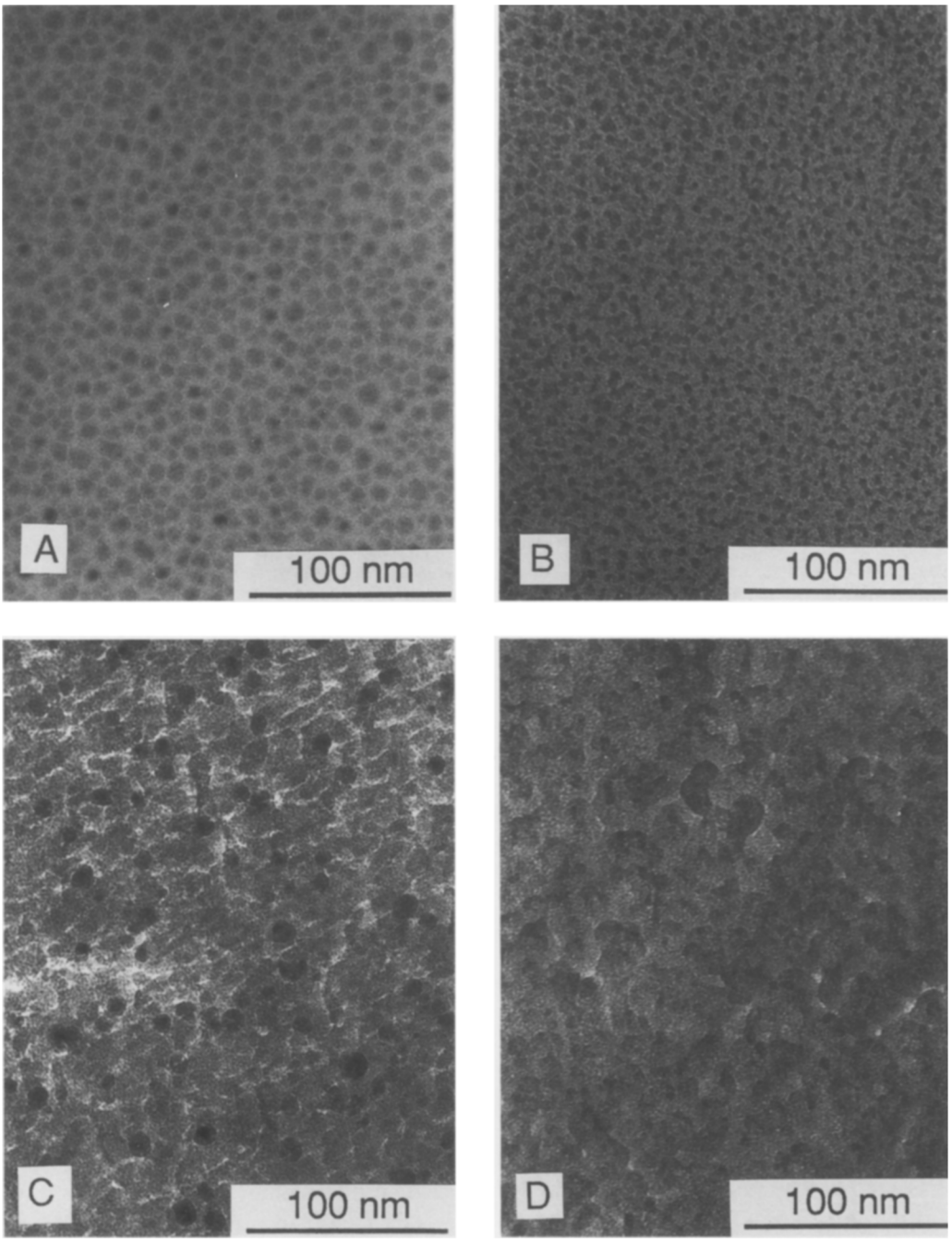

FIG. 9. Micrographs of the appearance of films illustrated in Fig. 5 after reduction in H_2 at 300°C for 4 h. Oxide supports are: A, SiO_2; B, NSI; C, NS68; D, Nb_2O_5. Ni particles are not discernable in D due to high contrast of the support.

ferent environments with silica. The crystallization of niobia is influenced by its mobility, which in turn affects the behavior of nickel supported on the four oxide thin films. We will discuss these observations in terms of the underlying oxide–oxide and oxide–metal interactions and how they could account for the chemical properties of the corresponding high-surface-area, supported-nickel samples.

Niobia mobility. The mobility of species in our oxide samples can be directly related to the phases observed. In previous work we have shown that H-Nb_2O_5 is the thermodynamically stable phase of niobia, while T(or TT)-Nb_2O_5 is metastable (*16*). From both our work and that of others in the literature, the occurrence of T-Nb_2O_5 in samples heated over about 500°C is indicative of some outside agent stabilizing this form against transformations to the more stable H-form. These stabilizers can be either interfacial in nature, such as a silica support in the case of our NSI sample, or bulk impurities, as chloride and fluoride (among others) are known to stabilize T- or B-Nb_2O_5 (*15, 26, 27*). In our samples we interpret the occurrence of T-Nb_2O_5 to arise from partial stabilization of niobia. In this case, niobia has sufficient mobility to crystallize from the amorphous as-deposited state, but crystallization is limited by the influence of a stabilizer. In contrast, the occurrence of H-Nb_2O_5 is interpreted as indicating the presence of highly mobile niobia, free to crystallize to the favored form without outside influence.

The above model for niobia mobility can now be applied to our thin film samples before nickel deposition. The mobility of niobia so established will be used to help explain the behavior of nickel supported on the thin films. The SiO_2 films, containing no niobia, can be considered the base case. Thus, behavior of nickel on the SiO_2 films can be expected to be "normal" in the sense that the support is inert. The NSI thin films, as previously investigated, contain T-Nb_2O_5 after calcination at (600,2,O) (*10, 14*). After reduction at (500,1,H), again only T-Nb_2O_5 was observed. The niobia on this film is considered to have limited mobility on the basis of these observations. The limited mobility is due, in part, to direct bonding of some niobia with the silica support forming a surface-phase, which in turn stabilizes additional niobia to the T- form (*10, 13*). However, some niobia in the NSI samples must be more mobile, as after longer heating times or for thicker films H-Nb_2O_5 is seen to form in addition to T-Nb_2O_5 (*10*). The limited mobility seen in the NSI films is due to a combination of interaction with the support and to a limited supply of niobia.

Similarly, niobia on the NS68 thin films has a limited mobility due to the presence of silica, which acts either as an interfacial or a bulk stabilizer. T-Nb_2O_5 was formed on NS68 after heating at (800,2,O) or (500,1,H), while temperatures of at least 1000°C are needed to form H-Nb_2O_5. The darker contrast areas appearing in Fig. 4A represent limited-mobility niobia beginning to crystallize to the T-form.

In contrast, the behavior of the niobia thin film was as expected from comparison with bulk niobia. Only the metastable low-temperature form, T-Nb_2O_5, was noted below temperatures of about 800°C, except for samples heated for longer times, where a higher temperature form developed. These results are in accordance with suggestions of such behavior made by Schafer *et al.* (*15*). However, when the Nb_2O_5 thin film is reduced at (500,1,H), crystals having the appearance of H-Nb_2O_5 are observed (Fig. 4B). While electron diffraction from these crystals was not strong enough to contribute intensity to diffraction patterns of the sample, their morphology is similar to H-Nb_2O_5 crystals identified previously (*10, 11*), and does not resemble crystals of other niobia phases (*15, 28*). As seen by the presence of H-Nb_2O_5, niobia is highly mobile on the niobia thin films. The extensive formation of pits on the Nb_2O_5 films during reduction confirms the presence of highly mobile niobia. Dumesic *et al.* observed the formation

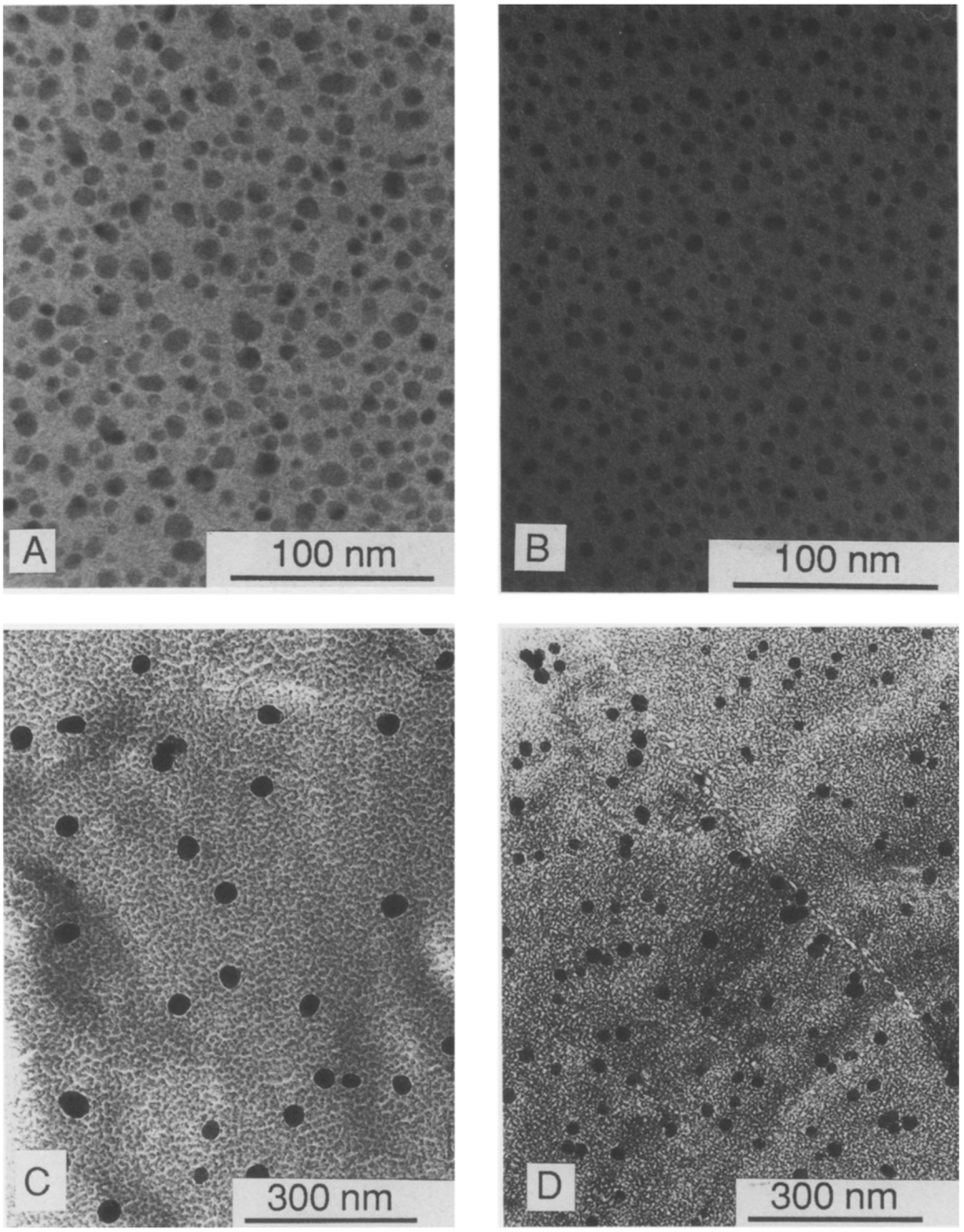

FIG. 10. Micrographs of the appearance of films illustrated in Fig. 5 after reduction in H_2 at 500°C for 4 h. Oxide supports are: A, SiO_2; B, NSI; C, NS68; D, Nb_2O_5. The support in D consists of two adjacent T-Nb_2O_5 crystals. Note that the scale in C and D is about one-third of that in A and B.

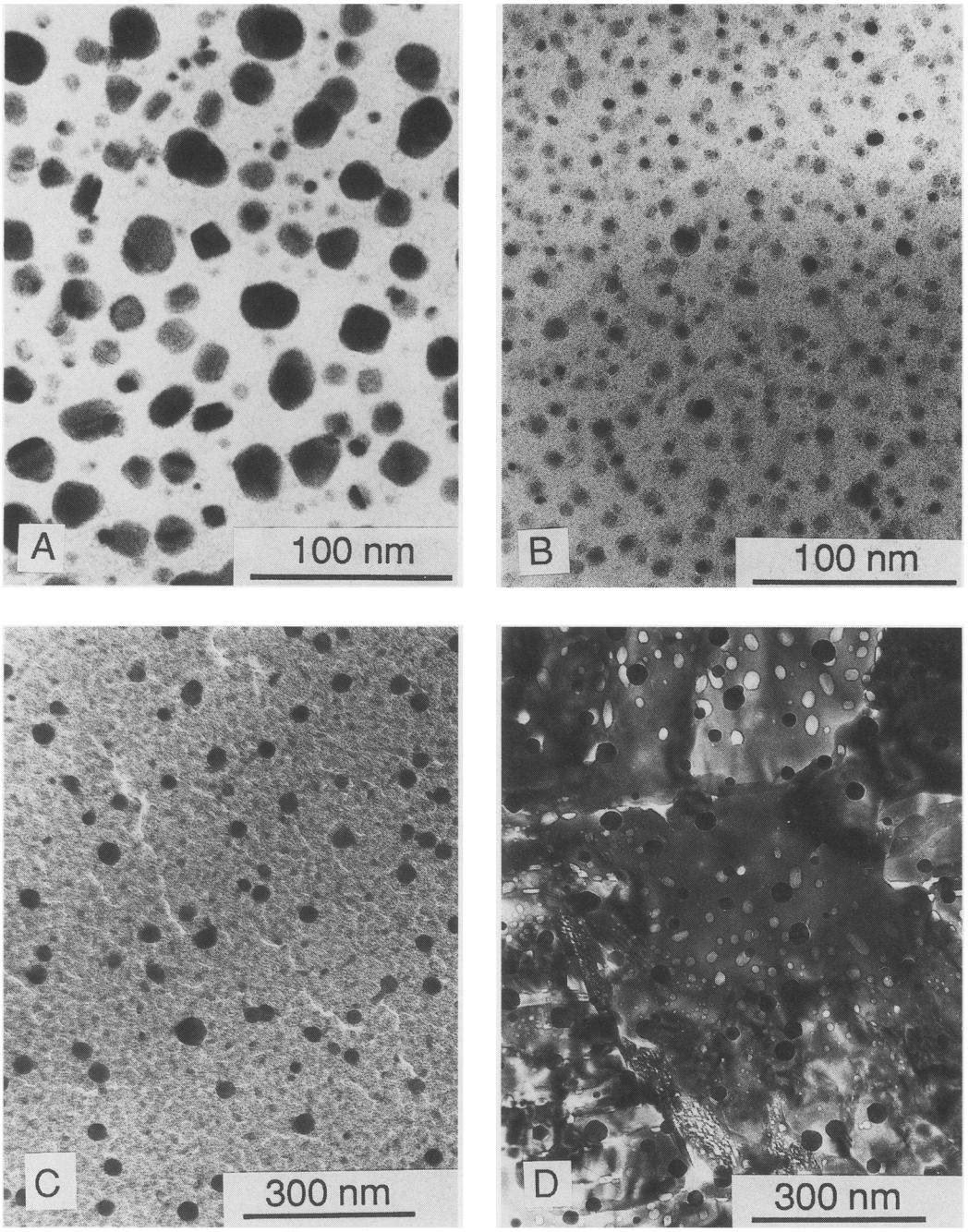

FIG. 11. Micrographs of the appearance of films illustrated in Fig. 5 after reduction in H_2 at 650°C for 4 h. Oxide supports are: A, SiO_2; B, NSI; C, NS68; D, Nb_2O_5. The support in C contains microcrystalline T-Nb_2O_5 crystals, while the support in D can be seen to consist of B-Nb_2O_5 as well as smaller T-Nb_2O_5 crystals. Note that the scale in C and D is about one-third of that in A and B.

TABLE 4

Phases Observed in Supported Nickel Thin Film Samples by Selected-Area Diffraction[a]

Treatment	SiO_2	NSI	NS68	Nb_2O_5
Ni, as deposited	NiO	NiO	A	NiO + T
(300,1,H)	Ni + NiO[b]	NiO	Ni	NiO[b]
(500,1,H)	Ni	Ni	Ni	Ni + T
(650,1,H)	Ni	Ni + NiNbO	Ni + T	T[c]
(300,4,H)	NiO + Ni	NiO	Ni	A
(500,4,H)	Ni	Ni	Ni	Ni + T[c]
(650,4,H)	Ni	Ni + NiNbO[b]	Ni + T	Ni + T[b] + NiNbO[b]

[a] Some phases abbreviated by: T, TT or T-Nb_2O_5; NiNbO, a phase similar to $Ni_{0.67}Nb_{11.33}O_{29}$ or $NiNb_2O_6$; A, amorphous.

[b] Weak.

[c] Strong.

of pits in TiO_2 thin films in contact with nickel. While they suggested that nickel facilitates reduction of titania, they reported that the formation of pits provides strong evidence for the ability of titania to migrate (*18*). Analogously, we consider the presence of pits in our reduced Nb_2O_5 films as strong evidence for high niobia mobility. The amount of pit formation seems to be more extensive when nickel is present, so while the presence of metal is not necessary for pits to form in reducible supports, it aids in pit formation.

Niobia is seen to occur in three states on the thin film samples, with corresponding degrees of mobility. Some niobia is bounded to the bulk, either to silica as in NSI or NS68, or to more niobia, as in the Nb_2O_5 thin film. This bonded niobia can be expected to have very low mobility. Some niobia has enough mobility to crystallize, but is still under some restraint, indicated by the eventual formation of T-Nb_2O_5, as was found in all three niobia-containing films. Niobia that eventually crystallized to H-Nb_2O_5 was the most mobile, as it crystallized under no restraints. In the presence of Ni, this range of mobility still occurs, with the added complication that the more mobile niobia species can show a greater degree of interaction with other species present; as a consequence, H-Nb_2O_5 was not observed in the supported nickel samples, instead this niobia interacted with the Ni particles, in some cases forming an observable nickel niobate. The next section will show how this range of niobia mobility and interactions with both Ni and SiO_2 affected the morphology of the samples.

Nickel behavior. As-deposited nickel, after exposure to atmosphere, was found to be poorly crystallized NiO. The oxidation of Ni is not surprising, as very small aggregates of the metal are pyrophoric. Ni on the

TABLE 5

Average Particle Diameters on Thin Film Supports[a]

Treatment	SiO_2	NSI	NS68	Nb_2O_5
(300,1,H)	6.6[b]	4.3[c,b]	9.4[c]	[d]
(500,1,H)	7.7[c]	7.2	23.3	16.7[c]
(650,1,H)	18.3	7.3[c,e]	25.8	23.9
(300,4,H)	7.4[c,b]	5.0[c,b]	8.8[c]	[d]
(500,4,H)	8.4[c]	6.6[c]	26.7	20.4[c]
(650,4,H)	17.5	7.3[c,e]	34.5[c]	29.3[c,e]

[a] From direct measurement of photographic enlargements of electron micrographs, diameters in nanometers. Particles are nickel unless otherwise specified.

[b] As NiO, at least in part.

[c] Smaller sized and/or irregularly shaped particles not clearly distinguishable from support and may not have been counted accurately.

[d] Particles not distinguishable from support.

[e] As Ni and nickel niobate.

high-silica-content thin films, SiO_2 and NSI, was difficult to reduce, forming the metal above 300°C, while Ni on NS68 and Nb_2O_5 was almost completely reduced by this temperature after only 1 h. A strong interaction between NiO and SiO_2 is responsible for this behavior. Other workers have observed the formation of nickel hydrosilicates under these conditions, these compounds being more difficult to reduce than NiO alone (*24, 29, 30*). The occurrence of NiO, as listed in Table 4, can be compared to Ni particle sizes given in Table 5. While Ni rapidly sintered to relatively large particles on NS68 and Nb_2O_5, the interaction of NiO and SiO_2 on the other two supports retarded the growth of Ni particles until reduction was complete and the interaction broken, taking temperatures above 500°C to do so. Ni on SiO_2 then crystallized to larger, well-formed crystals as seen in Figs. 8 and 11. In high-surface-area SiO_2-supported Ni prepared by precipitation of the Ni precursor, a strong chemical bond was formed between Ni and the support, eventually resulting in the stabilization of oxidized Ni on the surface and an increase in the difficulty of reduction. The reduced nickel particles then had about the same size distribution as particles of the oxidic precursor (*29, 30*). Only after reductions above 500°C were larger Ni particles seen (*30*). As these results are remarkably similar to the behavior of Ni on our thin films, perhaps a similar stabilization or interaction of nickel oxide with our SiO_2 support occurs.

Ni supported on Nb_2O_5 is known to exhibit strong metal–support interactions, one aspect of which is the flattening of the metal particles into a "pillbox" morphology (*1, 2*). A relatively large loading of metal or a large particle diameter, as in the Ni on our samples, can overcome the tendency toward spreading on the support. A similar finding was noted for Ni supported on TiO_2 after reduction at 500°C for 1 h. While small loadings of Ni had a flat morphology on TiO_2, Ni in larger loadings appeared more equidimensional (*8, 31*). Spreading may occur at higher temperatures or longer reduction times with increasing metal-reduced oxide interactions. The high mobility of niobia on this support leads not only to the strong metal–support interaction noted previously, but also to the formation of nickel niobate in our thin film samples.

NiO interacts with the SiO_2 component in the NSI samples in a fashion similar to that of the SiO_2 support. However, as reduction temperatures increase, NiO is reduced to Ni while Nb_2O_5 mobility and Nb_2O_5–Ni interactions increase. This behavior can be followed in Figs. 6B–8B and 9B–11B, as instead of forming larger and better-formed crystals, Ni particles on NSI remain small and become increasing irregular; eventually spreading is observed over the support with the appearance of easily detectable nickel niobate after reduction at 650°C. This spreading is clearly seen in Fig. 13, where irregularly shaped darker contrast nickel particles are surrounded by lighter contrast nickel niobate. The extent of nickel niobate formation in these thin films is limited by the availability of Nb_2O_5. No T- or H-Nb_2O_5 was noted, as was found on films similarly treated but without Ni, as all available Nb_2O_5 reacted with the more plentiful Ni.

Recently Arai *et al.* (*32*) reported an electron microscopy study of Ni on model TiO_2–SiO_2 surface oxides. Unlike Nb_2O_5 on our support, they noted that TiO_2 more evenly covered SiO_2, forming large islands of stabilized polycrystalline anatase. Their Ni sintered more rapidly on the surface oxide than on just SiO_2. In general, their results for Ni on the TiO_2–SiO_2 surface oxide were similar to those for Ni on a very thick layer of TiO_2 on SiO_2, which behaved like bulk TiO_2. As TiO_2 covered their SiO_2 more extensively, little if any NiO–SiO_2 interaction occurred, in contrast with our Nb_2O_5–SiO_2 surface oxide. The fact that their TiO_2 was more than a monolayer could also account for the different behavior observed for a high-surface-area Ni on TiO_2–SiO_2 sample (*6*).

Other than the thickness of the overlayer, we need to consider the preparation meth-

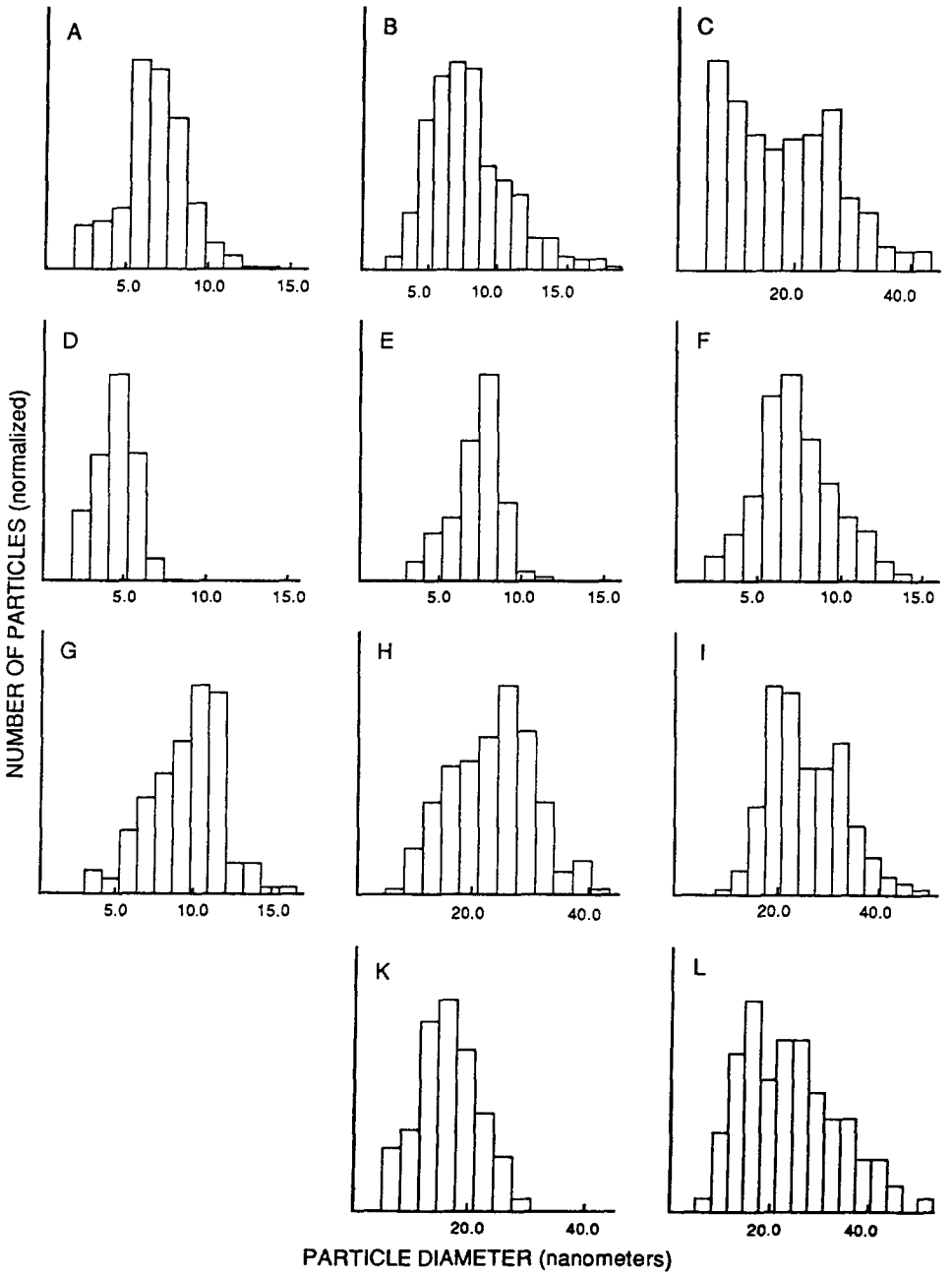

FIG. 12. Normalized nickel particle diameter histograms for samples heated in hydrogen for 1 h. A, (300,1,H)SiO_2; B, (500,1,H)SiO_2; C, (650,1,H)SiO_2; D, (300,1,H)NSI; E, (500,1,H)NSI; F, (650,1,H)NSI; G, (300,1,H)NS68; H, (500,1,H)NS68; I, (650,1,H)NS68; K, (500,1,H)Nb_2O_5; L, (650,1,H)Nb_2O_5.

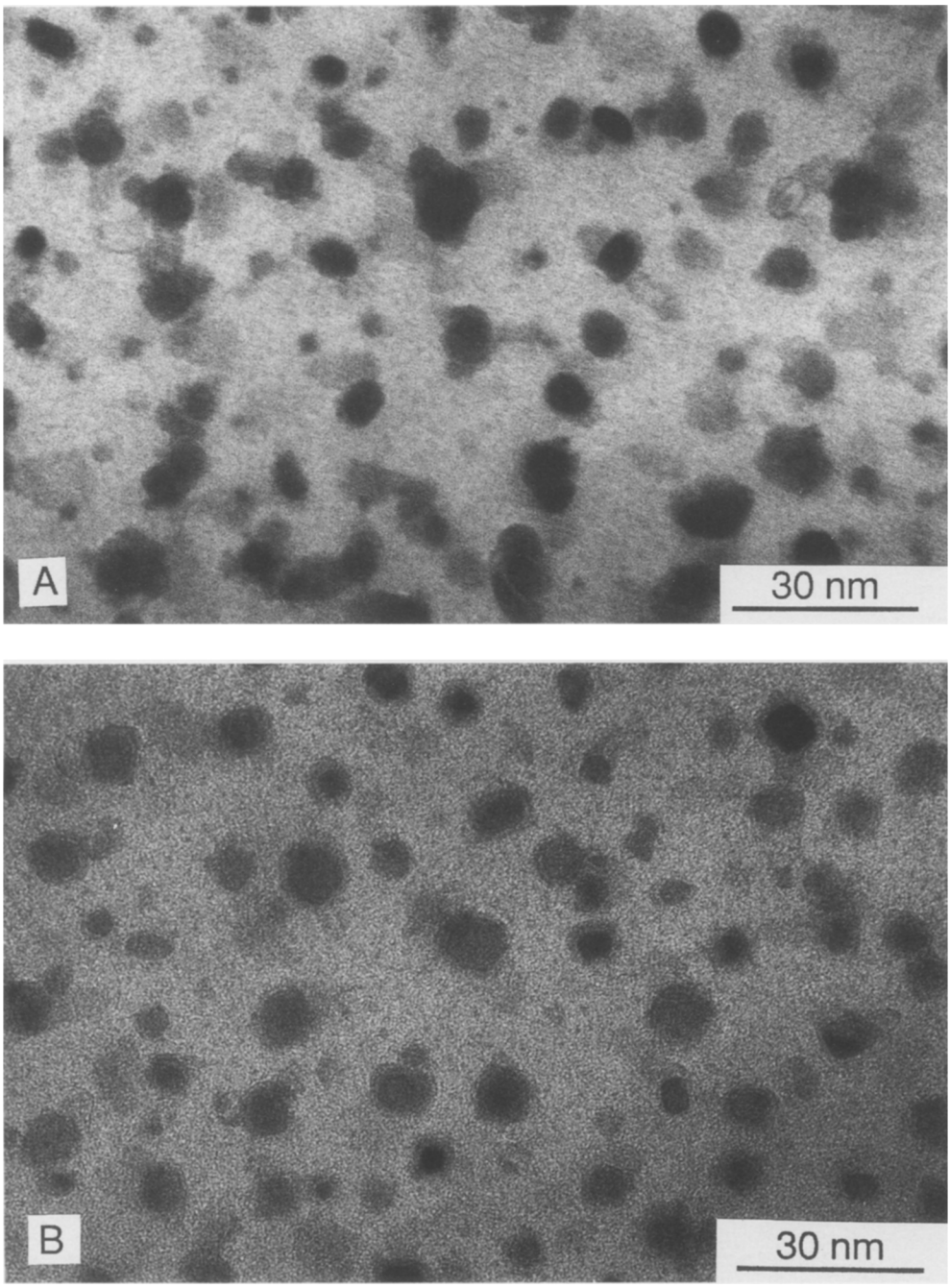

FIG. 13. Micrographs showing more clearly the formation around and the spreading from Ni particles of a phase that corresponds to nickel niobate on the NSI supports. Micrographs correspond to regions in Figs. 8B and 11B; A, reduced at 650°C for 1 hr; B, 650°C, 4 h.

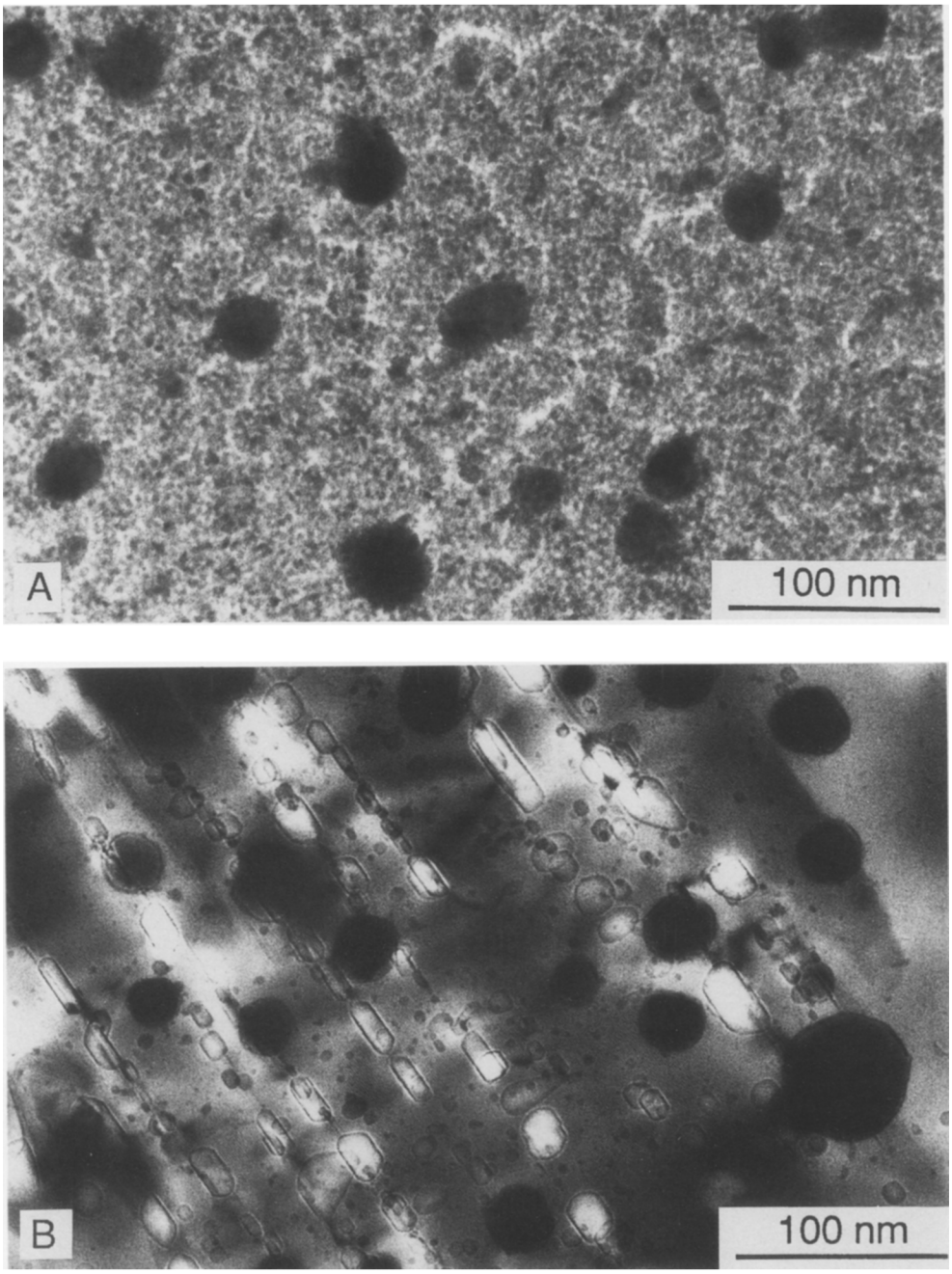

FIG. 14. Micrographs showing more clearly the morphology of Ni on NS68, A, and Nb_2O_5, B, supports after reduction at 650°C for 4 h. Pit formation on a single B-Nb_2O_5 (010) crystal is apparent in B.

ods in comparing thin-film and high-surface-area surface oxides. Our results (*10, 11*) and those on other oxide combinations (e.g., V_2O_5 on TiO_2, MoO_3 on γ-Al_2O_3) (*9, 33–35*) indicated that, in general, the supported oxide in a model system is less stable and so more mobile than that in the corresponding high-surface-area sample. This means, in our case, the observed metal–support interaction between Ni and NSI is likely to be stronger on the thin films, even though the qualitative features remain the same in both series of samples.

Finally, in comparison to the two single oxide supports, Ni on the mixed oxide support behaves in a more complicated fashion. Ni on NS68 shows no evidence of NiO–SiO_2 interaction, as the as-deposited NiO is easily reduced to the metal. Furthermore, the irregularly shaped T-Nb_2O_5 crystals observed on the reduced support (Fig. 4A) were not found on the supported Ni NS68 thin films. This absence suggests that any mobile niobia interacts with Ni. However, there is no detectable nickel niobate even after more extreme reduction on the NS68 supports.

Metal–support interactions. The physical characteristics of our thin films provide insight into the chemical properties of the corresponding high-surface-area samples listed in Table 1. We consider Ni on SiO_2 to be a base case in the sense that SiO_2 acts as an inert support. For Nb_2O_5 and NSI, interactions between the metal and support are evident in the different crystallization behavior of Nb_2O_5 with or without the presence of Ni, together with the direct identification of nickel niobate.

The formation of nickel niobate represents an extreme case of metal–support interactions. We showed previously (*36*) that there is a significant decrease in CO hydrogenation activity accompanying this compound formation on bulk niobia supports compared to that on NSI supports. Furthermore, the higher activity on NSI was ascribed to a more favorable distribution of the migrating suboxide species. In this study, we have shown that there is indeed a lower mobility of niobia in the NSI films due to a combination of interaction with the support and to a limited supply of niobia. These results are similar to those found for platinum supported on tungstena–silica (*37–39*) and for rhodium supported on lanthana–silica surface oxides (*40, 41*). In all cases, an oxide–oxide interaction limited the mobility of the supported oxide. It appears then a supported interacting oxide changes the extent but not the nature of the interaction.

Results in Table 1 show that Nb_2O_5/SiO_2 mixed oxides are also interacting supports for Ni but the interaction is of a different nature. Specifically, the CO hydrogenation activity decreases with respect to silica and there is no shift in selectivity toward higher hydrocarbons. We previously observed a similar trend in CO hydrogenation for Ni supported on TiO_2/SiO_2 mixed oxides and suggested that the coexistence of TiO_2 and SiO_2 in a chemically mixed system affects the interaction between Ni and TiO_2 (*42*).

Recall that on the NS68 thin film, Nb_2O_5 does not form a more stable phase even after heating to 800°C. This is evidence that niobia and silica are strongly interacting, even though some limited niobia mobility is observed. As silica does not crystallize under the conditions investigated, the mobility of silica could not be determined by the techniques used here. Nonetheless, the structure of the mixed oxide may be thought of as a loosely interconnected network, because, while silica is a network forming oxide, niobia is a network breaker (*43*). Sufficient niobia will effectively break most Si–O–Si linkages that may be present, creating what may be tetrahedral SiO_4 groupings or perhaps niobia–silica groupings within the mixed oxide. TiO_2/SiO_2 and Nb_2O_5/SiO_2 mixed oxides are similar in that both TiO_2 and Nb_2O_5 are network breakers and are both immiscible with SiO_2 (*44, 45*), so in both cases there is a driving force for oxide mobility in addition to that arising from gel degradation. Considering these facts, we speculate that the unusual chemical behavior of nickel on

mixed oxide supports after reduction at 500°C or higher may be due to a migrating species also. The identity of such a species is unknown, but one possibility, as mentioned above, is a niobia–silica grouping or silica alone. The migrating species cannot be niobia by itself, in view of the different activity and selectivity in CO hydrogenation and the lack of nickel niobate formation. In sum, the chemical evidence points to a physical blocking of nickel particle surfaces by a comparatively inert ad-species.

CONCLUSIONS

The use of thin films to interpret the behavior of corresponding high-surface-area materials, in this case nickel supported on SiO_2, Nb_2O_5, Nb_2O_5/SiO_2 mixed oxide, and Nb_2O_5–SiO_2 surface oxide, has been successfully demonstrated. These films enabled both a qualitative and quantitative analysis of the behavior of Ni on these supports. The morphology of Ni was found to depend on several chemical interactions, including interactions between NiO and SiO_2 during reduction, between Nb_2O_5 and SiO_2, affecting the mobility of niobia moieties which in turn affect Ni behavior, and between Nb_2O_5 and Ni, affecting the chemistry of the Ni.

Ni on SiO_2 was found to behave in a normal matter, although a NiO–SiO_2 interaction at lower reduction temperatures limited Ni particle sizes. Ni on Nb_2O_5 was found to behave according to the strong metal–support interaction model; at higher reduction temperatures, the interaction was strong enough to produce nickel niobate. Ni supported on a niobia surface oxide on silica behaved analogously to Ni on Nb_2O_5; however, the limited amount of mobile niobia present on the surface oxide prevented a full interaction from taking place while the presence of NiO–SiO_2 interactions served to limit Ni particle sizes. Ni on niobia/silica mixed oxide supports was found to have a morphological behavior similar to that of Ni on Nb_2O_5 but a differing chemical behavior. An ad-species that is not a reducible oxide moiety may be responsible for the physical and chemical behavior of nickel on mixed oxide supports.

ACKNOWLEDGMENTS

This work was supported by the Center for Study of Materials at Carnegie Mellon University under National Science Foundation Grant DMR-8521805 and by the Niobium Products Company, Inc. The authors thank Peter Burke at Carnegie Mellon University for supplying high-surface-area and bulk niobia samples and some data related to these samples.

REFERENCES

1. Stevenson, S. A., Dumesic, J. A., Baker, R. T. K., and E. Ruckenstein, Eds., "Metal–Support Interactions in Catalysis, Sintering, and Redispersion." Van Nostrand–Reinhold, New York, 1987.
2. Baker, R. T. K., Tauster, S. J., and Dumesic, J. A., Eds. "Strong Metal–Support Interactions." American Chemical Society, ACS Symposium Series, No. 298, 1986.
3. Ko, E. I., Bafrali, R., Nuhfer, N. T., and Wagner, N. J., *J. Catl.* **95,** 260 (1985).
4. Ko, E. I., Hupp, J. M., Rogan, F. H., and Wagner, N. J., *J. Catal.* **84,** 85 (1983).
5. Ko, E. I., Winston, S., Woo, J., *J. Chem. Soc. Chem. Commun.*, 740 (1982).
6. Ko, E. I., and Wagner, N. J., *J. Chem. Soc. Chem. Commun.*, 1274 (1984).
7. Takatani, S., and Chung, Y.-W., *J. Catal.* **90,** 75 (1984).
8. Raupp, G. B., and Dumesic, J. A., *J. Catal.* **97,** 85 (1986).
9. Hayden, T. F., and Dumesic, J. A., *J. Catal.* **103,** 366 (1987).
10. Weissman, J. G., Ko, E. I., and Wynblatt, P., *J. Catal.* **108,** 383 (1987).
11. Weissman, J. G., PhD dissertation, Carnegie Mellon University, 1987.
12. Weissman, J. G., Burke, P. A., Ko, E. I., and Wynblatt, P., *J. Chem. Soc. Chem. Commun.*, 329 (1989).
13. Burke, P. A., Weissman, J. G., Ko, E. I., and Wynblatt, P., *in* "Catalysis 1987" (J. W. Ward, Ed.), p. 457. Elsevier, Amsterdam/New York, 1988.
14. von Heimendahl, M., "Electron Microscopy of Materials." Academic Press, London, 1980.
15. Schafer, H., Gruehn, R., and Schulte, F., *Angew. Chem. Int. Ed. Engl.* **5,** 40 (1966).
16. Weissman, J. G., Ko, E. I., Wynblatt, P., and Howe, J., *Chemistry of Materials*, **1,** 187 (1989).
17. Ruckenstein, E., and Lee S. H., *J. Catal.* **104,** 259 (1987).
18. Dumesic, J. A., Stevenson, S. A., Sherwood, R. D., and Baker, R. T. K., *J. Catal.* **99,** 79 (1986).

19. JCPDS, Powder Diffraction File Nos. 32–694 and 27–892.
20. Hu, Z., Nakamura, H., Kunimori, K., and Uchijima, T., *J. Catal.* **112,** 479 (1988).
21. Marcelin, G., Ko, E. I., and Lester, J. E., *J. Catal.* **96,** 202 (1985).
22. Phadke, M. D., and Ko, E. I., *J. Catal.* **100,** 503 (1986).
23. Kim, K.-T., and Ihm, S.-K., *J. Catal.* **96,** 12 (1985).
24. Blackmond, D. G., and Ko, E. I., *Appl. Catal.* **13,** 49 (1984).
25. Burke, P. A., PhD dissertation, Carnegie Mellon University, 1989.
26. Kodama, H., Kikuchi, T., and Goto, M., *J. Less-Common Met.* **29,** 415 (1972).
27. Izumi, F., and Kodama, H., *Z. Anorg. Allg. Chem.* **440,** 155 (1978).
28. Ritschel, M., Oppermann, H., and Mattern, N., *Krist. Tech.* **13,** 1421 (1978).
29. Tamagawa, I., Oyama, K., Yamaguchi, J., Tanaka, H., Tsuiki, H., and Ueno, A., *J. Chem. Soc. Faraday Trans. 1* **83,** 3189 (1987).
30. Montes, M., Soupart, J.-B., deSaedeleer, M., Hodnett, B. K., and Delmon, B., *J. Chem. Soc. Faraday Trans. 1* **80,** 3029 (1984).
31. Jiang, X. Z., Stevenson, S. A., Dumesic, J. A., Kelley, T. F., and Casper R. J., *J. Phys. Chem.* **88,** 6191 (1984).
32. Arai, M., Nakayama, T., and Nishiyama, Y., *J. Catal.* **111,** 440 (1988).
33. Kang, Z. C., and Bao, Q. X., *Appl. Catal.* **26,** 251 (1986).
34. Vejux, A., and Courtine, P., *J. Solid State Chem.* **63,** 179 (1986).
35. Hayden, T. F., Dumesic, J. A., Sherwood, R. D., and Baker, R. T. K., *J. Catal.* **105,** 299 (1987).
36. Ko, E. I., Lester, J. E., and Marcelin, G., *ACS Symp. Ser.* **298,** 123 (1986).
37. Regalbuto, J. R., Fleisch, T. H., and Wolf, E. E., *J. Catal.* **107,** 114 (1987).
38. Regalbuto, J. R., Allen, C. W., and Wolf, E. E., *J. Catal.* **108,** 304 (1987).
39. Regalbuto, J. R., and Wolf, E. E., *J. Catal.* **109,** 12 (1988).
40. Alvero, A., Bernal, A., Carrizosa, I., and Odriozola, J. A., *Inorgan. Chim. Acta* **140,** 45 (1987).
41. Underwood, R. P., and Bell, A. T., *J. Catal.* **109,** 61 (1988).
42. Ko, E. I., Chen, J.-P., and Weissman, J. G., *J. Catal.* **105,** 511 (1987).
43. Fehlner, F. P., and Mott, N. F., "Oxidation of Metals," Vol. 2, p. 59. 1970.
44. Ibrahim, I., and Bright, N. F. H., *J. Amer. Ceram. Soc.* **45,** 221 (1962).
45. DeVries, R. C., Roy, R., and Osborn, E. F., *Trans. Brit. Ceram. Soc.* **53,** 531 (1954).
46. Chen, J.-P., PhD dissertation, Carnegie Mellon University, 1986.